

# Ordered Loop Current States in Bilayer Graphene

Lijun Zhu, Vivek Aji, Chandra M. Varma

Department of Physics and Astronomy, University of California, Riverside, CA 92521, USA

The zero gap non-interacting electronic structure of bilayer graphene is unstable to infinitesimal interactions. Indeed a gap is found in experiments but none of the states proposed so far is consistent with its properties. Here we show that a *Magneto-Electric* (ME) state is consistent with the experimental observations. This state breaks time-reversal symmetry through a pair of spontaneously generated current loops in each layer, and has odd-parity with respect to the two layers. We also show that such a state wins over the Haldane-type state with spontaneous quantum Hall effect (AHE) which has even parity, for large enough interactions and low enough temperature. We also propose further experiments to confirm this conclusion and the possibility that at higher temperatures the Haldane-type state is realized.

## I. INTRODUCTION

The non-interacting electronic state in bilayer graphene with AB (Bernal) stacking, See Fig. 1, has a pair of degenerate valence and conduction bands at two momentum points  $(0, \pm 4\pi/3\sqrt{3})$  in the Brillouin zone. The energy varies quadratically with the momentum about these points, in contrast with the linear dispersion in the single-layer graphene [1]. With hopping energy  $t_\perp$  between the stacking carbon atoms in different layers, the other two pairs of conduction and valence bands have energy at  $\pm t_\perp$  at the degeneracy points. Such a state with chemical potential at the charge neutrality point is unstable to infinitesimal electron-electron interactions. In weak-coupling approximation, in which the interaction energies are small compared to  $t_\perp$ , one may look for instabilities restricting the Hamiltonian to the set of lowest energy conduction and valence bands. In such a reduced basis, a wide variety of states, Charge Density Wave, Valley Density Wave, Spin-Density wave, Anomalous Hall State (AHE) [2–10], have been proposed as possible ground states. However, the conductance experiments [11–15], done with high mobility samples and with both a top and a bottom gate to ensure that the chemical potential is at the charge neutrality point [11], show an insulating state with characteristics which are not met by the proposed states. [17]

The two most important experimental findings can be summarized are that

(1) The state at charge neutrality shows a gap in two-terminal conductance measurements with a conductance  $G$  smaller than the limit of measurement  $\lesssim 10^{-2}e^2/h$  for voltage  $V < E_{g0}$ , above which

$$G \propto (V^2 - E_{g0}^2)^{-1/2}, \quad V \gtrsim E_{g0}, \quad (1)$$

with  $E_{g0} \approx 2meV$ .

(2) In small magnetic fields, the gap increases monotonically with a field, the conductance is consistent with a gap

$$E_g(H) \approx \sqrt{E_{g0}^2 + \omega_c^2}, \quad \omega_c = eB/m^*c \quad (2)$$

with  $m^* \approx (1/20)m$ , the free-electron mass.

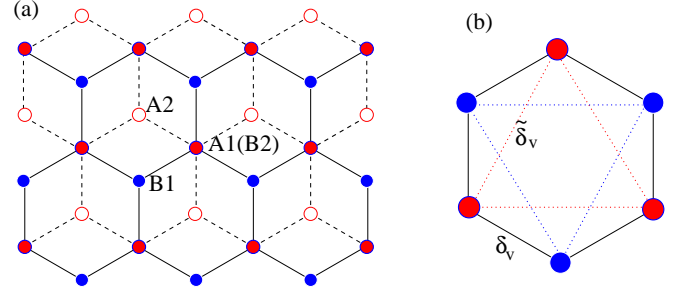


FIG. 1: (Color online) (a) Schematic of the bilayer lattice (top view). Bonds in layers 1 and 2 are indicated by solid and dashed lines, respectively. Here, A atoms in layer 1 (A1) and B atoms in layer 2 (B2) are stacked on top of each other. (b) is a unit cell for layer 1. Here  $\delta_v$  and  $\tilde{\delta}_v$  represent the bonds between the nearest (nn) and the next nearest (nnn) neighbors, respectively.

The Charge-Density wave, and Valley-Density States are not consistent with a gap; the AFM state has a gap above which the conductance has the form of Eq. (1), but it does not have field dependence of the gap of the form (2), (except in the unlikely case that conductance of only one layer is being measured). The AHE state does have a gap in the *bulk* and whose variation with field is also of the form (2). But it also has a surface band with a quantized Hall conductance of  $ne^2/h$  with  $n$  depending on the degeneracy, which in this case is 4. This contributes to the two probe conductance measurements and therefore is not consistent with the observations either.

An AHE state is possible if either inversion symmetry is preserved or if it is broken, the product of inversion and time-reversal is also broken [18, 19]. In bilayer graphene with AB stacking, the stacked atoms in each layer are at points of inversion, See Fig. (1). In this situation, AHE is possible only if two conditions are met: (1) the direction of the flux in the triangle formed by the stacked and the unstacked atoms in each layer is the same, (the magnitude is in general may be different). (2) the direction of flux in the triangle formed by the stacked (unstacked) atoms in layer 1 is the same as that of the unstacked (stacked) atoms in layer 2. The other three possibilities violate inversion with the product of inversion and time-

reversal preserved and therefore do not have an AHE. In the weak coupling approximation ( $V_{nnn} \ll t_\perp$ , where  $V_{nnn}$  is the next neighbor interaction), AHE is the only state accessible among these four. We show that when the coupling is larger ( $V_{nnn} > O(t_\perp)$ ), the ground state is the ME state, with a flux pattern depicted in Fig. (3d-f) and has properties consistent with the experiments.

## II. MODEL

The non-interacting model has a nearest neighbor hopping  $t$ , a next nearest neighbor hopping  $t_1$  and the hopping between the stacked carbon atoms  $t_\perp = t_{A1,B2}$ . We consider a nearest neighbor interaction parameter  $V_{nn}$  and a next nearest neighbor interaction parameter  $V_{nnn}$ , which controls the many-body effects. On-site interactions only renormalize the parameters for the states we consider and therefore will not appear. Other possible terms in the kinetic energy such as  $t_{A2,B1} \approx 0.3eV$  (the trigonal warping term) do not make any essential difference.

The Hamiltonian is

$$\begin{aligned} H &= H_1 + H_2 + H_{12} + H_{int} \\ H_l &= t \sum_{i,\delta_\nu} \left( a_{li}^\dagger b_{li+\delta_\nu} \right) + t_1 \sum_{l,\tilde{\delta}_\mu} \left( a_{li}^\dagger a_{li+\tilde{\delta}_\mu} \right) + h.c. \\ H_{12} &= t_\perp \sum_i a_{1i}^\dagger b_{2i} + h.c. \\ H_{int} &= V_{nn} \sum_{l,i,\delta_\nu} n_{li} n_{li+\delta_\nu} + V_{nnn} \sum_{l,i,\tilde{\delta}_\nu} n_{li} n_{li+\tilde{\delta}_\nu}. \end{aligned} \quad (3)$$

$l$  is the layer index taking the values (1,2),  $n_{li} = c_{nli}^\dagger c_{li}$  where  $c$  is the fermion operator,  $a_{li}$  or  $b_{li}$  and  $n_{li}$  the charge density operator. ( $\delta_1$  to  $\delta_3$ ) are the three vectors connecting the nearest neighbor sites on each layer and ( $\tilde{\delta}_1$  to  $\tilde{\delta}_6$ ) are the 6 vectors connecting the next nearest neighbor sites on each layer.

Estimates for the parameters extracted either from band structure calculations or deduced from experimental measurements are:  $t \approx 3eV$ ,  $t_\perp \approx 0.4eV$ ,  $t_1 = 0.1 - 0.3eV$ .  $t_1$  cannot be estimated accurately and the limits of the range quoted are from experiments and band-structure calculations respectively. The crystal structure yields an onsite potential difference between stacked and unstacked site of  $\Delta = 0.01$  eV. But as noted inversion through the stacked atom in each layer is preserved.

## III. MEAN FIELD ANALYSIS

We consider states that break time reversal symmetry through orbital loop-currents. In Appendix A, we discuss why symmetry breaking states generated due to  $V_{nn}$  need not be considered even though  $V_{nn} \approx 2V_{nnn}$ . Therefore

we confine our attention to symmetry breaking due to  $V_{nnn}$  and assume that  $V_{nn}$  only renormalizes the parameters used in the calculation. The mean field analysis of the model starts with the decomposition of the diagonal in spin part of the density interactions between sites as was done to derive time-reversal breaking ME states in cuprates [20]

$$\begin{aligned} n_{li} n_{lj} &= - \left( O_{li,j}^\dagger O_{li,j} / 2 + n_{li} + n_{lj} \right), \\ O_{li,j} &= \left( i c_{li}^\dagger c_{lj} + H.C. \right). \end{aligned} \quad (4)$$

The one particle terms can be dropped. Now a mean-field approximation is made with  $V_{ij} \langle O_{li,j} \rangle \equiv r$  for next nearest neighbor bonds ( $i,j$ ). This leads to a time-reversal breaking Hamiltonian for electrons with complex hopping between sites:

$$\begin{aligned} t_{ij} &\rightarrow t_{ij} + \left( V_l \langle c_{li}^\dagger c_{lj} + H.C. \rangle \right) \\ &\equiv t_{ij} + i r_{ij} \equiv \tilde{t}_{ij} \exp(i\phi_{i,j}), \end{aligned} \quad (5)$$

for  $r \ll t$ , as well as terms in energy of the form  $r^2/2V$ .  $r$  may now be determined by minimization of energy.

There are four kinds of states which can be generated through  $V_{nnn}$  which break time-reversal without breaking translational symmetry. They can be classified by the signs of the flux within different areas (triangles) enclosed by the next-nearest-neighbor bonds. (1) Within each layer, the triangles of A sublattice and B sublattice can have the same or opposite signs of flux (see Fig. 2). (2) Between two layers, the triangles of the unstacked atoms (B1, A2) centered at the stacked atoms (A1,B2) can have the same or opposite signs of flux as well [see Fig. 3(a-b,d-e)]. Of these the two states which break inversion through having flux in the stacked and unstacked triangle of atoms in a given layer in opposite direction [Fig. 2(b)] always have a higher ground state energy than the other two constructed from Fig 2(a) and will not be considered further. We are then left with two possibilities, with flux in the stacked and unstacked triangle of atoms in a given layer in the same direction. They can be further classified by the second condition, and are

- (i) The Haldane or AHE state of the bilayer in which the orientations of the flux in the loops atop each other in the two layers are the same. The flux patterns are shown in Fig. 3(a-c).
- (ii) The Magneto-electric (ME) phase with the opposite orientations of the flux in the loops atop each other in the two layers, Fig. 3(d-f). In both cases the net flux through a unit-cell is zero.

We calculate the ground states energy in mean-field in the space of all the four bands. We define  $r$  of Eq. (5) by using in it  $V = V_{nnn}$  and ( $i,j$ ) nearest neighbors for both stacked and unstacked atoms in the same layer. We find the leading dependence in energy on the order parameter

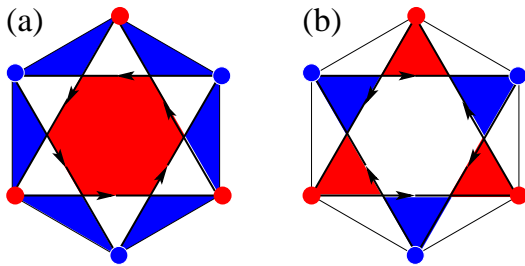


FIG. 2: The pattern of net fluxes in one layer (the top layer is illustrated as an example). The red and blue colors represent the positive (counterclockwise) and negative (clockwise) fluxes, respectively. For each layer, there are two possible loop-ordered states generated through  $V_{nnn}$ : the triangles enclosed by bonds connecting A1, B1 sublattices and with the same center have the same (a) or opposite (b) signs of fluxes. (a) corresponds to the Haldane's AHE flux pattern for a single-layer honeycomb lattice. Here, the inversion symmetry is preserved because the center of the honeycomb lattice is the inversion point. However, the inversion symmetry is always broken for (b).

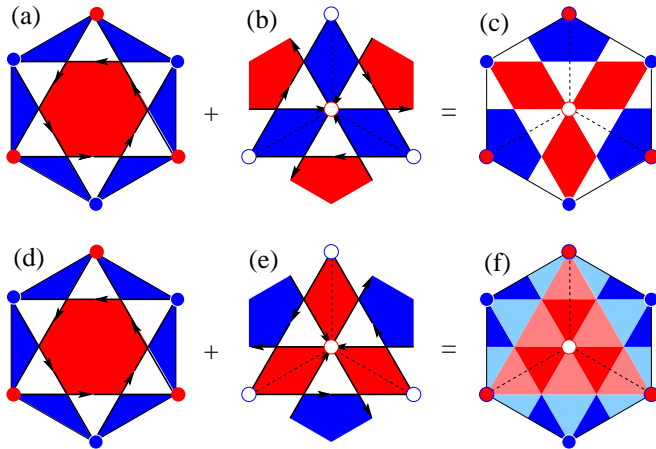


FIG. 3: The pattern of fluxes in the bilayer as viewed from above. (a-c) represent the AHE state while (d-f) represent the ME state, as discussed in the text. For each state, the flux patterns for the top layer (a and d), the bottom layer (b and e), and the net fluxes (c and f) are shown. The color representation is the same as in Fig. 2. In (f), we use light red (blue) to represent weaker strengths of fluxes compared to the regions with regular red (blue) colors.

$r$  for the AHE and the ME states to be, respectively,

$$E(r)_{ME}/t = \left( \frac{1}{2V_{nnn}} - 9.056 \right) r^2 + 228.5r^4$$

$$E(r)_{AHE}/t = \left( \frac{1}{2V_{nnn}} - 9.422 \right) r^2 + 306.4r^4. \quad (6)$$

Eq. 6 gives the interesting result that for  $V_{nnn} \gtrsim 0.05t$ , the magneto-electric phase has a lower ground state energy in such mean-field calculation. Eq. 6 also suggests that as temperature is decreased, the first state to arise through a transition with Ising symmetry is the AHE

state (with a first order transition), and then to the ME state at a lower temperature. We calculate the temperature dependence of the ground state energy, from which we estimate the transition temperature to the ME state is  $T_c \sim 10^{-2}t$  (for  $V_{nnn} = 0.1t$ ). The transition temperature to the AHE state is 5% higher. The value of the transition temperature is expected to be depressed from these estimates by fluctuations. The one-particle excitations in AHE state have a direct gap while in the ME state have an indirect gap with features at higher energy, shown in Fig. 5 which should be looked for in experiments.

#### IV. NUMERICAL ANALYSIS

To examine the property of the time-reversal symmetry breaking state with an applied magnetic field, we diagonalize the mean-field Hamiltonian with a magnetic field on a finite lattice of the size of the magnetic translation. We calculate both the density of states and the various topological properties of the AHE and the ME states, such as the edge states and the Chern numbers, when they exist. The details are given in the Appendices. The important results are stated here.

For the AHE state, any finite order parameter  $V_{nnn}$  will open up a gap  $\Delta \approx 6\sqrt{3}r$ . As verified by the edge modes, see Fig. 4, it has a quantized Hall conductance at zero magnetic field. We calculated the Chern numbers for the 4 bands, which are  $C = (0, 2, -2, 0)$  in sequence of energy. This gives a quantized Hall conductance  $\sigma_{xy} = 4e^2/h$  for  $r < O(t_\perp)$ . For  $r > O(t_\perp)$ , the Chern numbers are  $C = (2, 0, 0, -2)$  instead.

The ME state has an indirect gap (see Fig. 4) only for  $r > O(t_\perp)$ . For small  $r$ , one obtains a semi-metal. The insulating ME state is not accessible within the two-band low-energy approximation. As shown in Fig. 4, the edge modes do not cross; so the ME state does not carry a net Hall current at zero field. The direct gaps produce further sharp features in one-particle excitations which should be looked for to confirm the existence of this state, as shown in Fig. 5.

We expect that the density of states of the ME state at the edge of the gap becomes much sharper because the excitonic effects are not included in our calculation.

We now examine the property of ME state in a finite magnetic field. The density of states is shown in Fig. 5. Unlike the AHE state, where the lowest Landau level is pinned to the edge of the gap [21], the lowest Landau level(s) shifts up in energy, leading to a larger gap. The magnetic field dependence of the gap is shown in Fig. 6, and agree with experiments when extrapolated to low fields of the experiments.

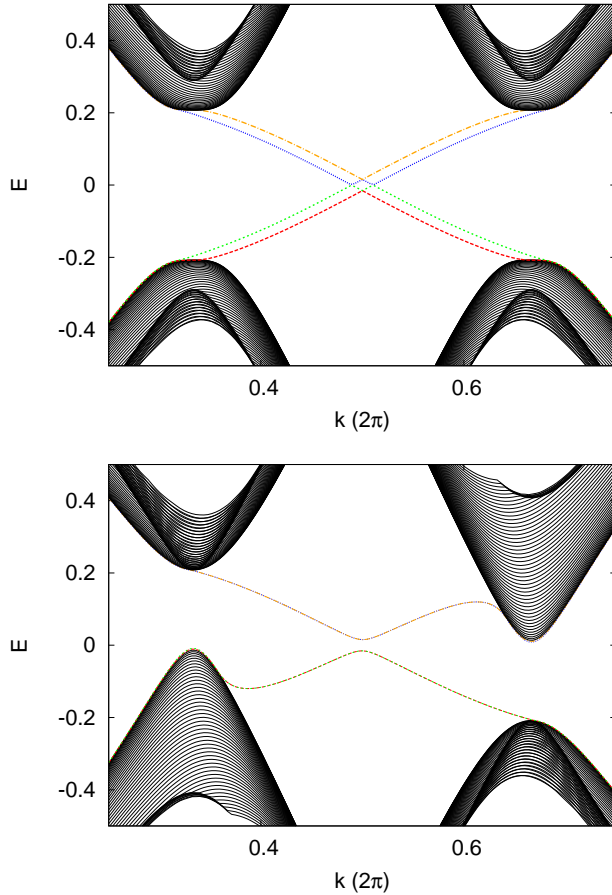


FIG. 4: The bandstructures with edge modes (assuming an open boundary condition along the zig-zag edge) for AHE (top panel) and ME (bottom panel) states. For the non-interacting bilayer graphene, there are four bands: two low-energy valence and conduction bands touch each other at two momentum points K and K'. The other two high-energy bands are split with a scale of  $t_{\perp}$ . In the AHE state, band gaps are opened at both K and K' due to the order parameter  $r$ ,  $\Delta \approx 6\sqrt{3}r$ . In the ME state, there are also direct band gaps at K and K',  $\Delta_d \approx 3\sqrt{3}r$ . But the center of the direct gaps shift in different directions of energy for K and K'. When  $\Delta_d \gtrsim t_{\perp}$ , an indirect gap opens. For illustration purposes, we take  $t_{\perp} = 0.2t$  and  $r = 0.04t$  here, which are slightly bigger than realistic values.

## V. CONCLUSION

The principle experimental observation of an insulating state at charge neutrality in bilayer graphene, with a gap growing monotonically with a magnetic field, is the signature of a novel state of matter. We have shown that these results are only consistent with a state that breaks both the time-reversal and inversion symmetries, but not translational invariance. When a Haldane phase is realized in each layer, the even parity combination of two layers (i.e. AHE state) has edge modes and finite conductivity, while the odd parity combination (i.e ME

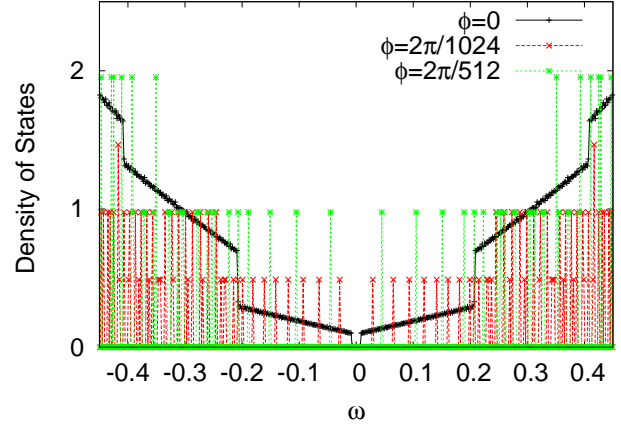


FIG. 5: The density of state of ME state without and with a magnetic field. Here  $t_{\perp} = 0.2t$  and  $r = 0.04t$ . The zero-field DOS has been multiplied by a factor 5. The magnetic field strength is specified by the flux per unit cell  $\phi = 2\pi/M$  where  $M$  is an integer (see Appendix B for more details).

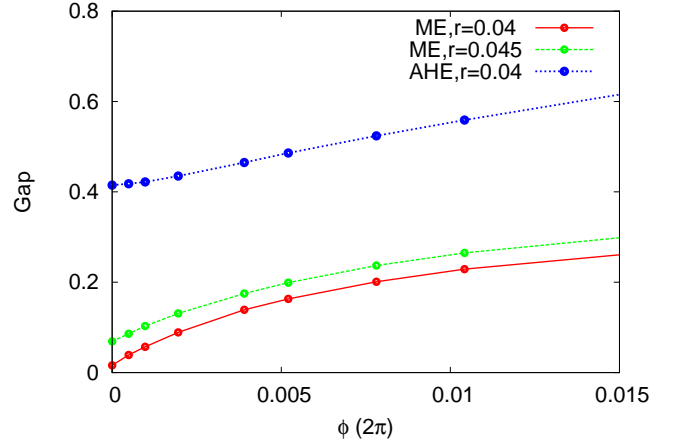


FIG. 6: The gap as a function of the external magnetic field. Here  $t_{\perp} = 0.2t$ . The magnetic field strength is in terms of the flux per unit cell  $\phi = 2\pi/M$ , and  $M$  has been chosen as 128, 256, ..., 2048.

state) does not. We have shown that the ME state is the ground state of interacting bilayer graphene, and its properties are in agreement with those of the observed insulating state. We suggest conductance experiments at higher biases to confirm the ME state through observations of the jumps in the density of states of Fig. 5.

We have also considered the possibility of the actual realization of the Haldane AHE state in a single layer graphene by our mean-field procedure. Again the nearest neighbor interactions are ineffective and need a very large value to get any change in symmetry but a next nearest neighbor interaction  $V_{nnn}$  approx larger than about  $0.1t$  leads to the Haldane state. This requires a dielectric constant to be smaller than about 10, which appears to be close to what experiments report.

## Acknowledgements

We acknowledge extensive discussions with Professor C.N. Lau. L.Z. also acknowledges discussions with Professor Donna Sheng. This research was partially supported by NSF grant DMR-0906530 (L.Z. and C. M. V.), and UCR initial complement(V.A.).

## Appendix A: Ordered Loop Current States generated through $V_{nn}$

For the nearest neighbor interaction  $V_{nn}$ , the generated loop currents flow around the perimeter of a hexagonal cell with net flux. If we allow flux (positive or negative) in any unit-cell, we run into the problem of frustration of an Ising model in a triangular lattice. This in general is not a possible ground state because unlike with spins, alternate arrangements with lower energy are possible. The simplest is a  $\sqrt{3}a \times \sqrt{3}a$  structure of hexagons depicted in Fig. 7 in which a hexagonal cell with zero net flux is surrounded by six hexagonal cells, each with a Kekule pattern of currents in the links with alternate net positive and negative flux. This state breaks the translational symmetry while the unit cell is enlarged to include  $3 \times 3$  unit cells of a translational invariant honeycomb lattice.

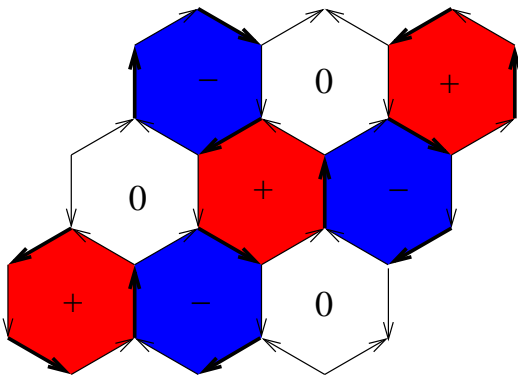


FIG. 7: A possible ordered loop-current state generated through  $V_{nn}$ . Only one layer is shown. The red, blue and white colors represent the net positive (clockwise), negative (anticlockwise), and zero fluxes in a hexagonal cell.

We assume that the flux pattern in the top layer follows Fig. 7, which takes a sequence  $(+, -, 0)$  from left to right. The bottom layer could follow the same pattern, or takes another pattern  $(-, +, 0)$ . Therefore, there are two types of ordered loop current states (the other combinations are equivalent to either of these two states by rotation). We carry out a mean-field calculations on the ground states energy for these states, and find that the state with different patterns for two layers are lower in energy. This lower energy state is allowed only if  $V_{nn} \gtrsim 2.06t$ , i.e., be comparable to the bandwidth. The reason is that such a state does not have a “nesting” periodicity and therefore does not use singularity in the joint

density of states.

## Appendix B: Numerical Methods

The mean-field Hamiltonian of the ordered loop current states can be readily diagonalized for each momentum point  $(k_x, k_y)$ . However, to examine their properties under an applied magnetic field, as well as the topological properties such as the edge modes, we also carry out a real-space calculation.

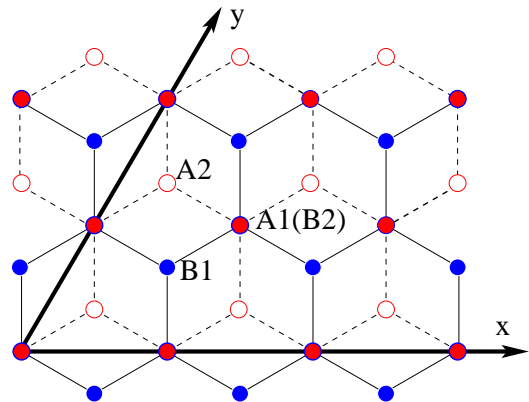


FIG. 8: The bandstructures with edge modes (assuming an open boundary condition along the zig-zag edge) for AHE (top panel) and ME (bottom panel) states. Here we take  $t_{\perp} = 0.2t$  and  $r = 0.04t$ .

Following a common numerical practice for honeycomb lattices, we describe the bilayer graphene by a  $N_x \times N_y$  lattice, with four atoms on each lattice site (see Fig. 8). The real-space coordinations of each atom (and the momentum) in the orthogonal x-y axis can be easily obtained from this “deformed”-lattice representation.

The effect of an external magnetic field can be captured by imposing a phase to the hopping term to each bond  $t_{ij} \rightarrow t_{ij}e^{i\int \mathbf{A} \cdot d\mathbf{x}}$ . We adopt the Landau gauge  $A_y = -Bx$  to take advantage of the translational invariance along  $y$ -direction. For the periodic boundary condition, we commonly take the flux due to the external magnetic field in a unit cell to be  $\phi = 2\pi/M$ , where  $M$  is an integer proportional to  $N_x$ .  $M = 1000$  is equivalent to a magnetic field strength  $B \approx 30T$  for graphene systems.

In general, we choose periodic boundary conditions along both directions (a torus). This provides a verification of our momentum-space calculations for the zero-field. For the edge modes calculation, we choose an open boundary along  $x$ -axis, which corresponds to a cylinder with the zigzag edge.



## Appendix C: Additional Results

### 1. Density of States

In Fig. 9, we show the density of states (DOS) for the ME state with various values of the order parameter  $r$ . We also show the result for the non-interacting case as well. For  $r = 0$ , the DOS at  $\omega = 0$  is finite, which is due to the parabolic dispersion  $E \sim k^2$ . There is a sudden jump of DIS at  $\omega \approx \pm t_\perp/2$ , which is the energy scale of the gap between top two valence bands (bottom conduction bands). When  $r$  is small, the conduction band at K point and the valence band at K' point have overlaps in energy. Therefore, it remains a semi-metal state. A full gapped state happens when  $r \gtrsim t_\perp/(3\sqrt{3})$ .

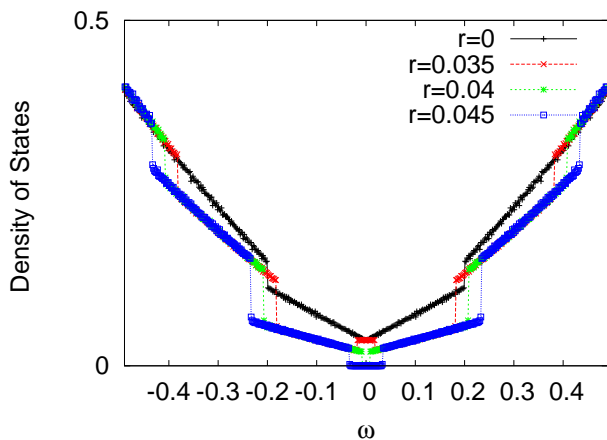


FIG. 9: The density of states for the ME state. Various values of the loop current order parameter are shown. The non-interacting case  $r = 0$  is also shown in comparison. Here  $t_\perp = 0.2t$ .

### 2. Chern numbers

In the main paper, we have shown the topological properties of the AHE and ME states by showing their edge

modes, calculated by assuming a periodic boundary condition along y-axis and an open boundary condition along x-axis. Judging from the crossed edge modes, we learn the AHE state indeed has a finite Hall conductance at zero-field. Similarly, the ME state does not have any Hall effect at zero-field.

This topological property can also be checked from the Chern numbers. The Chern number for a given band is defined as

$$C_n = \int_{BZ} \frac{d^2k}{(2\pi)^2} \hat{z} \cdot \frac{\partial \Psi_n^*(\mathbf{k})}{\partial k_x} \times \frac{\partial \Psi_n(\mathbf{k})}{\partial k_y}, \quad (C1)$$

where  $\Psi_n(\mathbf{k})$  is the wavefunction for  $n$ -band. The Hall conductance is given by  $\sigma_{xy} = Ce^2/h$ . We calculate the Chern numbers in a momentum-space algorithm, by summing the Berry curvature in small areas ( $\Delta k_x, \Delta k_y$ ).

For the AHE state, any finite order parameter  $r$  will open up a gap. We find the Chern numbers for the 4 bands are  $C = (0, 2, -2, 0)$  in sequence of energy, i.e, the valence and conduction bands away from fermi energy do not carry any Chern numbers. However, when  $r \gtrsim t_\perp$ , the Chern numbers become  $C = (2, 0, 0, -2)$  instead. In either case, a finite Hall conductance is a robust feature.

For the ME state, an indirect gap is open only for a finite order parameter  $r \gtrsim t_\perp$ . However, as long as the four bands do not touch with each other (having direct band gaps), the Chern number calculation is robust. We find the Chern numbers for the four bands of the ME state are all zero, indicating a none-quantum Hall state. When  $r \gg t_\perp$ , we find the Chern numbers become  $C = (1, -1, 1, -1)$ . In this limit, each layer is a Haldane state while  $t_\perp$  only acts as a perturbation, slightly splitting the stats from two layers. Still, there is no Hall effect near the Fermi energy.

### 3. Edge Modes in a finite magnetic field

In the main paper, we have shown the edge modes for AHE and ME states at zero-field. For completeness, we also show the edge modes in a finite external magnetic field, in Fig. 10.

- 
- [1] McCann, E. & Fal'ko, V. I. Landau-level degeneracy and quantum hall effect in a graphite bilayer. *Phys. Rev. Lett.* **96**, 086805 (2006).
  - [2] Nandkishore, R. & Levitov, L. Flavor symmetry and competing orders in bilayer graphene. Preprint at <http://arxiv.org/abs/1002.1966v1> (2010).
  - [3] Zhang, F., Jung, J., Fiete, G. A., Niu, Q. A. & MacDonald, A. H. Spontaneous quantum Hall states in chirally stacked few-layer graphene systems. *Phys. Rev. Lett.* **106**, 156801 (2011).
  - [4] Jung, J., Zhang, F. & MacDonald, A. H. Lattice theory of pseudospin ferromagnetism in bilayer

graphene: competing interaction-induced quantum Hall states. *Phys. Rev. B* **83**, 115408 (2011).

- [5] Zhang, F., Min, H., Polini, M. & MacDonald, A. H. Spontaneous inversion symmetry breaking in graphene bilayers. *Phys. Rev. B* **81**, 041402 (R) (2010).
- [6] Lemonik, Y., Aleiner, I. L., Toke, C. & Fal'ko, V. I. Spontaneous symmetry breaking and Lifshitz transition in bilayer graphene. *Phys. Rev. B* **82**, 201408 (2010).
- [7] Vafeek, O. & Yang, K. Many-body instability of Coulomb interacting bilayer graphene: renormalization group approach. *Phys. Rev. B* **81**, 041401 (2010).
- [8] Castro, E. V., Peres, N. M. R., Stauber, T. & Silva,

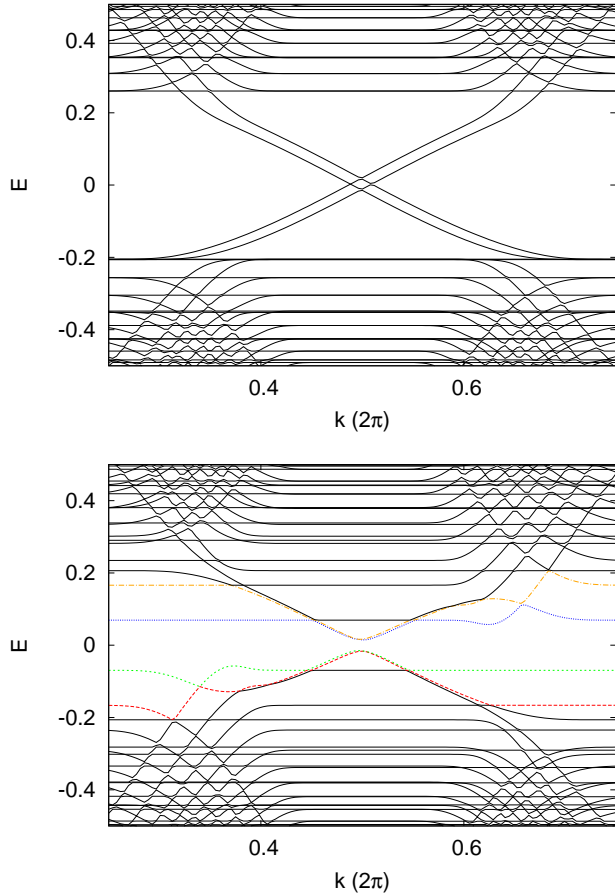


FIG. 10: The edge modes for AHE (top panel) and ME (bottom panel) states at a finite magnetic field. Here  $t_{\perp} = 0.2t$ ,  $r = 0.04t$  and  $\phi = 2\pi/256$ .

N. A. P. Low-density ferromagnetism in biased bilayer graphene. *Phys. Rev. Lett.* **100**, 186803 (2008).

- [9] Kharitonov, M. Canted antiferromagnetic phase of the  $\nu = 0$  quantum Hall state in bilayer graphene. Preprint at <http://arxiv.org/abs/1105.5386> (2011).
- [10] Zhang, F. & MacDonald, A. H. Distinguishing spontaneous quantum Hall states in graphene bilayers. Preprint

at <http://arxiv.org/abs/1107.4727> (2011).

- [11] Velasco Jr., J., Ling, J., Bao, W., Lee, Y., Kratz, P., Aji, V., Bockrath, M., Lau, C. N., Varma, C., Stillwell, R., Smirnov, D., Zhang, F., Jung, J. & MacDonald, A. H. Transport spectroscopy of symmetry-broken insulating states in bilayer graphene. Preprint at <http://arxiv.org/abs/1108.1609v1> (2011).
- [12] Feldman, B. E., Martin, J. & Yacoby, A. Broken-symmetry states and divergent resistance in suspended bilayer graphene. *Nature Physics* **5**, 889 (2009).
- [13] Weitz, R. T., Allen, M. T., Feldman, B. E., Martin, J. & Yacoby, A. Broken-symmetry states in doubly gated suspended bilayer graphene. *Science* **330**, 812-816 (2010).
- [14] Freitag, F., Trbovic, j., Weiss, M. & Schönenberger, C. Spontaneously gapped ground state in suspended bilayer graphene. Preprint at <http://arxiv.org/abs/1104.3816v2> (2011).
- [15] Hone, J., Kim, P., Deshpande, V., Chen, C. & Koshino, M., unpublished (2012). The results are presented in ([http://online.kitp.ucsb.edu/online/graphene\\_c12/hone/](http://online.kitp.ucsb.edu/online/graphene_c12/hone/)).
- [16] Mayorov, A. S., Elias, D. C., Mucha-Kruczynski, M., Gorbachev, R. V., Tudorovskiy, T., Zhukov, A., Morozov, S. V., Katsnelson, M. I., Falko, V. I., Geim, A. K. & Novoselov, K. S. Interaction-Driven Spectrum Reconstruction in Bilayer Graphene, *Science* **333**, 860 (2011).
- [17] We concentrate here on the experiments reported in Ref. [11] because the three other references [12–15] have similar results but with a higher conductance in the gap. One group [16] obtains rather different results. The origin of the difference from those of the other four groups is not clear.
- [18] Sun, K. & Fradkin, E. Time-reversal symmetry breaking and spontaneous anomalous Hall effect in fermi fluids. *Phys. Rev. B* **78**, 245122 (2008).
- [19] He, Y., Moore, J. & Varma, C. M. Berry phase and anomalous Hall effect in a three-orbital tight-binding Hamiltonian. Preprint at <http://arxiv.org/abs/1112.6393> (2011).
- [20] C.M. Varma, Pseudogap Phase and the Quantum-Critical Point in Copper-Oxide Metals, *Phys. Rev. Letters*, **83**, 3588 (1999).
- [21] Haldane, F. D. M. Model for a quantum Hall effect without Landau levels: condensed-matter realization of the “Parity Anomaly”. *Phys. Rev. Lett.* **61**, 2015 (2006).